Neutron Measurement of Clustering in the Alloy CuNi†

B. MOZER* AND D. T. KEATING
Brookhaven National Laboratory, Upton, New York 11973

AND

S. C. Moss
Massachusetts Institute of Technology, Cambridge, Massachusetts 02139

(Received 12 June 1968)

Measurements have been made of the cluster diffuse neutron scattering from a polycrystalline sample of $Cu_{0.525}Ni^{62}_{0.475}$. This isotope and composition are ideal for such measurements since the effective scattering length for the Bragg reflections and for the temperature-diffuse and Huang scattering from static displacements is zero, while that for the cluster scattering is 0.811×10^{-12} cm. The short-range order parameters α_1 through α_9, representative of the system at approximately 550°C, were determined by a least-squares fit to the scattering data. $\alpha_1=0.121$, while all other α's are less than $\frac{1}{3}\alpha_1$. Magnetic scattering effects in this sample are too small to have been detected within the accuracy of our measurements. Using an approximate theory of Clapp and Moss relating the short-range order parameters and pairwise interaction energies, first- and second-neighbor interaction energies of −0.0130 to −0.0122 eV and +0.0073 to +0.0078 eV are determined. From these, a critical temperature for phase separation of 233 to 263°C is predicted, which is in reasonable agreement with that extrapolated from thermodynamic data of Rapp and Maak and of Oriani and Murphy.

INTRODUCTION

A NULL sample (zero Bragg scattering) of copper-nickel isotopically enriched in nickel-62 was prepared by one of us for the purpose of determining the phonon frequency distribution.[1] Several neutron diffraction patterns made of the alloy to check on homogeneity and null condition revealed a pronounced oscillation in the incoherent background, the Laue monotonic scattering, as shown in Figs. 1 and 2. These patterns are typical of alloy clustering, the tendency of an atom to surround itself with neighbors of the same species.[2] Indeed, there have been a number of measurements on Cu-Ni alloys that are indicative of segregation. In calculating the Ni-Cr-Cu phase diagram, Meijering[3] predicted a miscibility gap in the alloy Cu-Ni closing at a critical point of 177°C. Oriani and Murphy[4] measured a positive enthalpy of formation, which, according to the quasi-chemical model, is indicative of clustering. Rapp and Maak[5] concluded from their activity measurements, which showed a positive deviation from Raoult's law, that a miscibility gap should occur at about 300°C and should be similar in shape to that of the Au-Ni system.[6] Köster and Schüle[7] concluded from their measurements of electrical resistivity and Hall constant that clustering occurs somewhere between 300 to 650°C. Ryan *et al.*[8] have inferred that either clustering or a miscibility gap exists from their measurements of the magnetic susceptibility on neutron-irradiated Cu-Ni alloys. More recent measurements of electrical resistivity on quenched and slow-cooled Cu-Ni alloys by Schüle and Kehrer[9] and on neutron-irradiated samples by Ascoli[10] have led these investigators to conclude that the alloy segregates.

From an experimental viewpoint our sample is ideal for measuring the cluster diffuse neutron scattering. The isotopic enrichment should increase the ratio of the cluster scattering per atom of sample to the coherent scattering per atom to $\sim9.6\times10^3$. For x rays this ratio is only $\sim3.0\times10^{-4}$. X-ray measurements of clustering on polycrystalline samples are always plagued by a rather unfavorable ratio,[11–15] and Flinn *et al.*[15,16] incorrectly concluded that the Au-Ni system exhibits short-range order partly because of this.[17] Because so few diffraction studies on segregating fcc systems[13–15] have been made, our sample was so ideally suited for such a study, and there is interest in Cu-Ni alloys in particular, we decided to make several accurate measurements of the cluster scattering from our sample. We believe that the short-range order parameters deter-

† Work performed under the auspices of the U. S. Atomic Energy Commission.

* Present address: Inorganic Materials Division, National Bureau of Standards, Washington, D. C. 20234.

[1] B. Mozer (to be published).

[2] B. E. Warren and B. L. Averbach, *Modern Research Techniques in Physical Metallurgy* (American Society for Metals, Cleveland, Ohio, 1953), p. 95.

[3] J. L. Meijering, Acta Met. **5**, 257 (1957).

[4] R. A. Oriani and W. K. Murphy, Acta Met. **8**, 23 (1960).

[5] R. A. Rapp and F. Maak, Acta Met. **10**, 63 (1962).

[6] L. Seigle, M. Cohen, and B. L. Averbach, Trans. AIME **194**, 1320 (1952).

[7] W. Köster and W. Schüle, Z. Metallk. **48**, 592 (1957).

[8] F. Ryan, E. Pugh, and R. Smoluchowski, Phys. Rev. **116**, 1106 (1959).

[9] W. Schüle and H. P. Kehrer, Z. Metallk. **52**, 168 (1961).

[10] A. Ascoli, *Radiation Damage in Solids II* (International Atomic Energy Agency, Vienna, 1962), p. 105.

[11] J. M. Dupouy and B. L. Averbach, Acta Met. **9**, 755 (1961).

[12] P. S. Rudman, Acta Met. **12**, 1381 (1964).

[13] P. S. Rudman and B. L. Averbach, Acta Met. **2**, 576 (1954).

[14] R. Sundahl, J. Silversten, and T. Chen, J. Appl. Phys. **36**, 1223 (1965).

[15] P. A. Flinn, B. L. Averbach, and Morris Cohen, Acta Met. **1**, 644 (1953).

[16] B. L. Averbach, P. A. Flinn, and Morris Cohen, Acta Met. **2**, 92 (1954).

[17] S. C. Moss and B. L. Averbach, in *Small-Angle X-Ray Scattering*, edited by H. Brumberger (Gordon and Breach, Science Publishers, Inc., New York, 1967), p. 335.

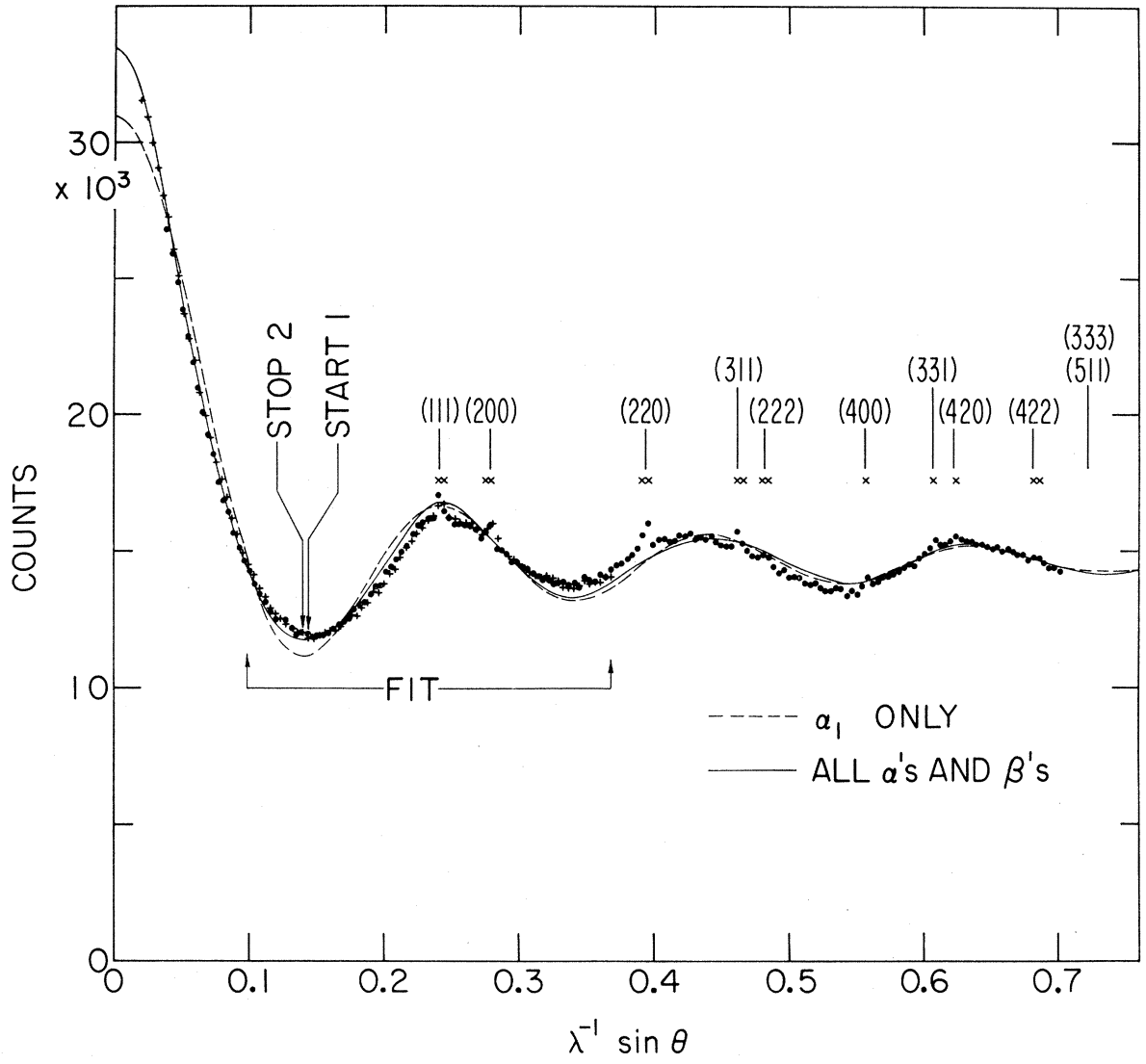

FIG. 1. Cluster scattering from two thicknesses of CuNi alloy, furnace-cooled from 1021°C. The pattern has been corrected for air scattering and to the condition of normal incidence and unit transmission. The data points indicated by pulses were taken with 1.951-Å neutrons, those with the solid circles with 1.024-Å neutrons, and the data matched as described in the text. The Bragg positions are indicated, the dashed curves is the least-squares fit with α_1 only, and the solid curve is the fit with the first nine α's and first five β's.

mined from this sample are an accurate description of the clustering in our sample at ~550°C. The uncertainty in the temperature is due to the quenching of the sample but this is only of the order of 50°C. We have related these short-range order parameters to first- and second-neighbor pairwise interaction energies of −0.0130 to −0.0122 eV and +0.0073 to +0.0078 eV, respectively. We have also related them to a predicted critical temperature of from 233 to 263°C, which is in reasonable agreement with that extrapolated from thermodynamic data.

SAMPLE PREPARATION

The sample was prepared from isotopically enriched nickel metal (batch No. 1460a) supplied from Oak Ridge National Laboratories. The assayed isotopic abundances in atomic percent were Ni^{58} 0.34%, Ni^{60} 0.48%, Ni^{61} 0.12%, Ni^{62} 99.06%, and Ni^{64} <0.05%. The major chemical impurities were Zn <0.2% and Th <0.2%. To ensure removal of nonmetallic impurities the coarse nickel powder was cold-pressed into a briquette and sintered in flowing H_2 for 5 h at 950°C. The sintered briquette was then melted into a button in an arc furnace in an atmosphere of 100 mm of argon. This button was then combined with 99.999% copper metal by melting and remelting in the arc furnace for a total of six melts. The final sample weighed 94.55 g and its composition was $Cu_{0.525}Ni_{0.475}$. The sample was then rolled to a thickness of ~0.071 in. for a reduction of about 6 and cut into two equal parts. The sample was

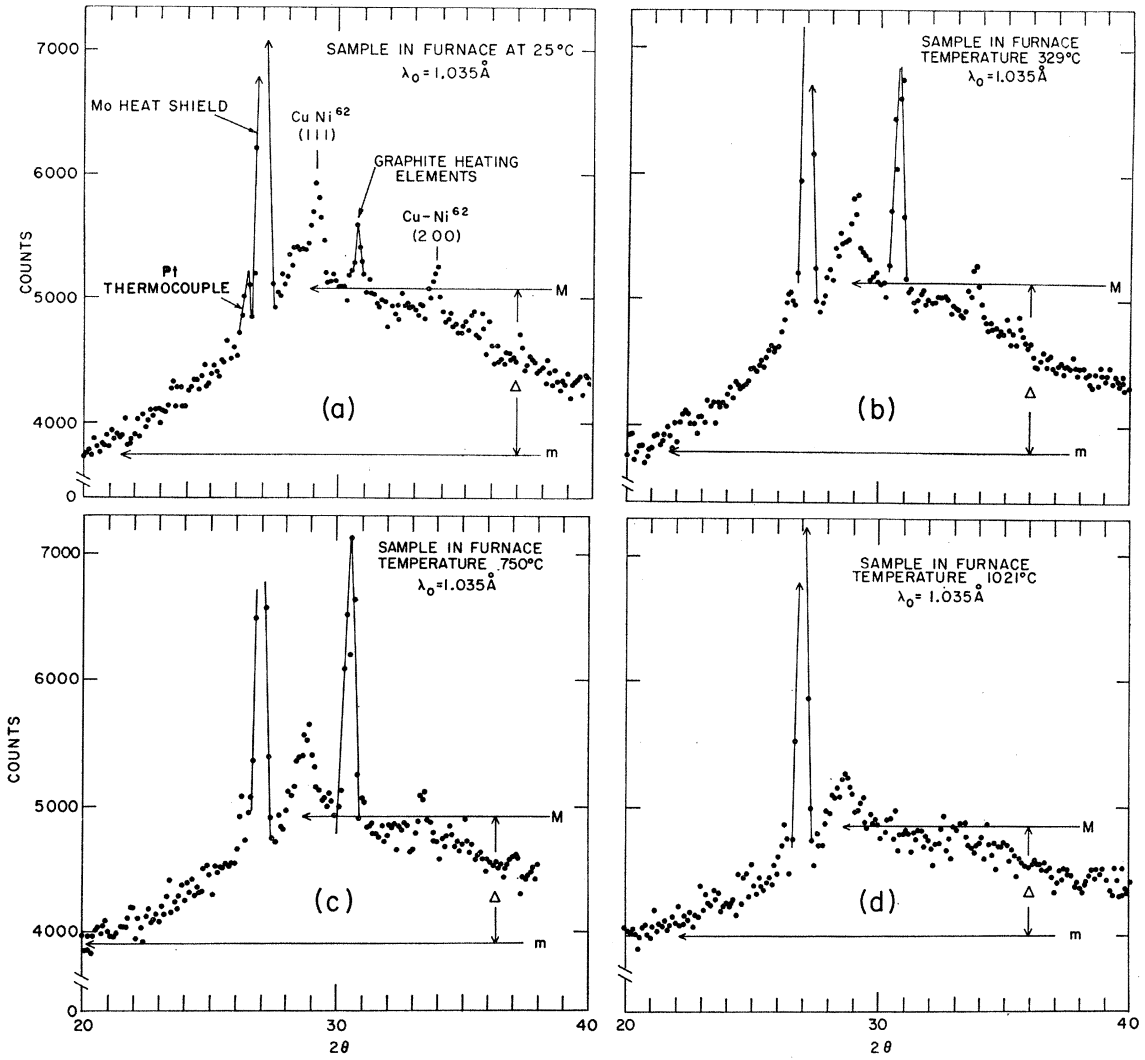

FIG. 2. The uncorrected scattering as a function of temperature from two thicknesses of CuNi alloy in high-temperature furnace: (a) 25°C, (b) 329°C, (c) 750°C, and (d) 1021°C. $\Delta = M - m$, the difference in the maximum and minimum of the cluster scattering.

then annealed for 3 h at ~1050°C. Following this, 24-h diffraction patterns were made at 4°K and at 2°K in an attempt to detect any long-range magnetic scattering. Then, consecutive patterns in Figs. 2(a)–2(d), each of 24-h duration, were made and the sample was furnace-cooled after the final 1021°C run. The investigation of the clustering presented here is on the sample as furnace-cooled.

DIFFRACTION THEORY AND EXPERIMENTAL PARAMETERS

We review briefly some of the pertinent quantities that enter into the analysis of the cluster diffuse scattering from a binary alloy. While most of these quantities are familiar to x-ray diffractionists, there are some terms that are unique to neutron measurements. We used the following expression for the diffuse scattering per atom of our sample:

$$I_D = I_M + M_{\mathrm{Cu}} I_{\mathrm{Cu}}^{\mathrm{inc}} + M_{\mathrm{Ni}} I_{\mathrm{Ni}}^{\mathrm{inc}} + M_{\mathrm{Ni}} I_{\mathrm{Ni}}^{\mathrm{PM}} + I_{\mathrm{SE}} + I_{\mathrm{SRO}}. \quad (1)$$

The first four terms in Eq. (1) arise in neutron measurements, and are the multiple scattering, spin isotope incoherent scattering, and paramagnetic scattering. M_{Cu} and M_{Ni} are the atomic fractions of copper and nickel. We have used Vineyard's[18] calculation for the multiple scattering in transmission when the angle of incidence equals the angle of transmission, which was the geometry of our experiment:

$$I_M = \frac{(\sigma_S/\sigma_T)(B/A)}{1-(\sigma_S/\sigma_T)(B/A)} \langle I_1 \rangle, \quad (2)$$

where σ_S is the scattering cross section of the sample,

[18] G. H. Vineyard, Phys. Rev. **96**, 93 (1954).

σ_T is the total cross section of the sample, and (B/A) is the ratio of the 2nd to 1st scattering coefficients, which is a function of $\tau=\sigma_T\rho_0/\rho_T N_v t$, where ρ_0/ρ_T is the ratio of the sample density to the theoretical density, $\langle I_1\rangle$ is the average first-order scattering, N_v is the theoretical atom density, and t is the thickness. The first-order scattering is very nearly isotropic in our case and the average first-order scattering was taken to be

$$\langle I_1\rangle=M_{\mathrm{Cu}}M_{\mathrm{Ni}}(\bar{b}_{\mathrm{Cu}}-\bar{b}_{\mathrm{Ni}})^2+M_{\mathrm{Cu}}I_{\mathrm{Cu}}{}^{\mathrm{inc}}+M_{\mathrm{Ni}}I_{\mathrm{Ni}}{}^{\mathrm{inc}}+M_{\mathrm{Ni}}I_{\mathrm{Ni}}{}^{\mathrm{PM}}, \quad (3)$$

where $\bar{b}_{\mathrm{Cu}}$ and $\bar{b}_{\mathrm{Ni}}$ are the average scattering length of the copper and nickel isotopes which constituted our sample.

The isotope incoherence was calculated from

$$I_i{}^{\mathrm{inc}}=\sum_{j=1}^{n}\sum_{k>j}^{n} m_j m_k(b_j-b_k)^2, \quad (4)$$

where i stands for Cu or Ni, m_j and b_j are the fraction and scattering length of the jth isotope, and n is the total number of isotopes in the ith element.

For want of a better estimate of the nickel paramagnetic scattering we write

$$I_{\mathrm{Ni}}{}^{\mathrm{PM}}=\tfrac{2}{3}p^2, \quad (5)$$

where $p=(\gamma e^2/mc^2)(\frac{1}{2}\langle\eta_\beta\rangle)f(\kappa)$, the quantity e^2/mc^2 is the scattering length of a Thompson electron, γ is the magnetic moment of a neutron in nuclear magnetons, $\langle\eta_\beta\rangle$ is the average number of Bohr magnetons per nickel atom, and $f(\kappa)$ is the magnetic form factor of nickel. Using Mook's[19] value of $p=0.155\times10^{-12}f(\kappa)$, we calculate $I_{\mathrm{Ni}}{}^{\mathrm{PM}}=0.016\times10^{-24}f^2(\kappa)$. This is probably an upper limit for the nickel paramagnetic scattering in our alloy, since upon substituting copper atoms for nickel, electrons are added into the vacant states of the nickel $3d$ band.[20] Thus, alloying should reduce $\langle\eta_\beta\rangle$ and hence the paramagnetic scattering. Accordingly, we have ignored any paramagnetic scattering effect.

The short-range order scattering is given by

$$I_{\mathrm{SRO}}=M_{\mathrm{Cu}}M_{\mathrm{Ni}}(\bar{b}_{\mathrm{Cu}}-\bar{b}_{\mathrm{Ni}})^2\times\Big[1+\sum_{i=1}^{\infty}C_i\alpha_i e^{-2B\gamma_i[(\sin\theta)/\lambda]^2}(\sin\kappa r_i)/\kappa r_i\Big], \quad (6)$$

where i is the shell index, C_i is the coordination number (number of atoms) in the ith shell, α_i is the short-range order parameter of the ith shell,[2] B is the Debye parameter, γ_i is the fraction of $2B$ effective for the ith neighbors,[21] and $\kappa=(4\pi\sin\theta)/\lambda$, where θ is half the scattering angle and λ the neutron wavelength. B was determined directly from the normalized experimental[1] frequency distribution $g(\nu)$ from[22]

$$B=\frac{h}{M}\int_0^\infty g(\nu)\coth\left(\frac{h\nu}{2kT}\right)\frac{d\nu}{\nu}, \quad (7)$$

where h is Planck's constant, $M=104.2\times10^{-24}$ g is the mean atomic mass of our alloy, ν is the frequency, k is Boltzmann's constant, and $T=300$°K is the temperature at which the measurement of $g(\nu)$ and the cluster scattering were done. Equation (7) gave a value of $B=0.4961$ Å^2 and a Debye characteristic temperature of 338.4°K. Assuming that the dispersion is that of a simple linear chain,[21] the γ's in Table I were determined.

TABLE I. Calculated γ_i's for linear chain dispersion.

i	1	2	3	4	5	6	7	8	9
γ_i	0.725	0.858	0.856	0.852	0.867	0.890	0.907	0.918	0.920

Following Warren *et al.*,[23] the size-effect scattering is given by

$$I_{\mathrm{SE}}=-M_{\mathrm{Cu}}M_{\mathrm{Ni}}(\bar{b}_{\mathrm{Cu}}-\bar{b}_{\mathrm{Ni}})^2\times\sum_{i=1}^{\infty}C_i\beta_i e^{-2B\gamma_i[(\sin\theta)/\lambda]^2}[(\sin\kappa r_i)/\kappa r_i-\cos\kappa r_i], \quad (8)$$

where

$$\beta_i=\left(\frac{1}{\eta-1}\right)\left\{-\left(\frac{M_{\mathrm{Cu}}}{M_{\mathrm{Ni}}}+\alpha_i\right)\epsilon_{\mathrm{CuCu}}{}^i+\left(\frac{M_{\mathrm{Ni}}}{M_{\mathrm{Cu}}}+\alpha_i\right)\eta\epsilon_{\mathrm{NiNi}}{}^i\right\}, \quad (9)$$

and $\eta=\bar{b}_{\mathrm{Ni}}/\bar{b}_{\mathrm{Cu}}$ and $\epsilon_{\mathrm{CuCu}}{}^i$ and $\epsilon_{\mathrm{NiNi}}{}^i$ are the fractional change in the ith interatomic distance when both sites are occupied by copper and nickel, respectively. While this expression has enjoyed reasonable success in explaining observed diffraction phenomena, it is inconsistent with the expression given by Borie.[24,25] Borie's expression depends both upon the difference in scattering lengths and the mean scattering length $(M_{\mathrm{Cu}}\bar{b}_{\mathrm{Cu}}+M_{\mathrm{Ni}}\bar{b}_{\mathrm{Ni}})$ and for our sample Borie's expression vanishes.

There are other scattering processes that depend upon the mean scattering length of the sample, such as the coherent phonon scattering and Huang scattering,[24,25] which for our sample are negligibly small and are not considered in Eq. (1).

In the preceding expressions we used what seemed to be the best available values of the parameters involved. We took the following values for scattering lengths: $\mathrm{Ni}^{58}=1.480\pm0.008$,[26] $\mathrm{Ni}^{60}=0.282\pm0.002$,[27] $\mathrm{Ni}^{61}=0.760\pm0.006$,[28] $\mathrm{Ni}^{62}=-0.850\pm0.018$,[26] $\mathrm{Cu}^{63}=0.672\pm0.015$,[29]

[19] H. A. Mook, Phys. Rev. **148**, 495 (1966).
[20] N. F. Mott and H. Jones, *The Theory and Properties of Metals and Alloys* (Dover Publications, Inc., New York, 1958), p. 192.
[21] C. B. Walker and D. T. Keating, Acta Cryst. **14**, 1170 (1961).
[22] M. Blackman, in *Encyclopedia of Physics*, edited by S. Flügge (Springer-Verlag, Berlin, 1955), Part I, Vol. 7, p. 325.
[23] B. E. Warren, B. L. Averbach, and B. W. Roberts, J. Appl. Phys. **22**, 1493 (1951).
[24] B. Borie, Acta Cryst. **10**, 89 (1957).
[25] B. Borie, Acta Cryst. **12**, 280 (1959).
[26] W. C. Koehler, E. O. Wollan, and C. G. Shull, Phys. Rev. **79**, 395 (1950).
[27] G. Caglioti, M. J. Cooper, and V. J. Minkiewicz, J. Appl. Phys. **38**, 1245 (1967).
[28] S. S. Sidhu and K. D. Anderson, Phys. Rev. **156**, 1225 (1967).
[29] D. T. Keating, W. J. Neidhardt, and A. N. Goland, Phys. Rev. **111**, 261 (1958).

$Cu^{65}=1.109\pm0.019$,[29] and $Cu=0.790\pm0.023$,[29] all in units of 10^{-12} cm. We then derived the following quantities: $\bar{b}_{Ni}=(-0.835\pm0.018)\times10^{-12}$ cm and $M_{Cu}\bar{b}_{Cu}+M_{Ni}\bar{b}_{Ni}=(0.0183\pm0.0148)\times10^{-12}$ cm; $I_{Cu}{}^{inc}=0.0408\pm0.0045$, $I_{Ni}{}^{inc}=0.0275\pm0.0006$, $M_{Cu}M_{Ni}\times(\bar{b}_{Cu}-\bar{b}_{Ni})^2=0.6583\pm0.0236$, and $\langle I_1\rangle=0.6927\pm0.0237$, all in units of 10^{-24} cm^2; and $\sigma_S=8.7052\pm0.2978$ b. We measured the transmission of two thicknesses of our alloy at 1.024, 4.04, and 6.30 Å and found the values 0.66602, 0.40970, 0.28310. We calculated from measured values of the cell edge, $a_0=3.589$ Å, the measured $\rho_0/\rho_T=0.98368$, and the measured thicknesses $t_1=0.18207\pm0.00127$ cm and $t_2=0.17978\pm0.0127$ cm, the cross sections at these three wavelengths. Assuming the cross section of our alloy to be "$1/V$" and that the cross section at $\lambda=0$ was the calculated σ_S, we least-squares fitted these cross sections to find $\sigma_T=(8.31383+5.15896\lambda)$ b or 13.595 b at 1.024 Å. This gave the values $\tau_1=0.21060$ for the first thickness, $\tau_2=0.20795$ for the second thickness, and $\tau_{1+2}=0.41856$ for the two thicknesses together. We then took $(B/A)_1=(B/A)_2=0.258$ and $(B/A)_{1+2}=0.401$ in Eq. (2), from which $(I_M/\langle I_1\rangle)_1=(I_M/\langle I_1\rangle)_2=0.19808$ and $(I_M/\langle I_1\rangle)_{1+2}=0.34570$. Thus, the multiple scattering at a wavelength of 1.024 Å was appreciable.

The diffuse counting rate at the angle 2θ, $y_D(2\theta)$, is given by

$$y_D(2\theta)=KN_vI_D(2\theta). \tag{10}$$

Denoting the Bragg scattering, above the diffuse background, by $y_{hkl}(2\theta)$, then the angular integration

$$\int_{-\infty}^{\infty}y_{hkl}(2\theta)d(2\theta)=KjQ_{hkl}/8\pi\sin\theta, \tag{11}$$

defines the integrated intensity. In Eq. (11), j is the multiplicity and Q_{hkl} is the integrated reflecting power[30] with

$$Q_{hkl}=\frac{\lambda^3N_C{}^2F_{hkl}{}^2e^{-2B[(\sin\theta)/\lambda]^2}}{\sin2\theta}, \tag{12}$$

where N_C is the number of cells per unit volume and F_{hkl} is the structure factor. The constant of proportionality, K, in Eqs. (10) and (11) is given by

$$K=RI_0(\rho_0/\rho_T)Atwh/r^2, \tag{13}$$

where R is the ratio of the counter efficiency to the monitor efficiency, I_0 is the incident intensity in neutrons cm^{-2} sec^{-1}, A is the area of the incident beam, t is the sample thickness, w is the effective slit width, h is the effective slit height, and r is the sample-to-counter distance.

Equation (10) was put in the form

$$y_D(2\theta)=A_0+\sum_{i=1}A_ie^{-2B\gamma_i[(\sin\theta)/\lambda]^2}(\sin\kappa r_i)/\kappa r_i+\sum_{i=1}B_ie^{-2B\gamma_i[(\sin\theta)/\lambda]^2}\cos\kappa r_i \tag{14}$$

and the A's and B's determined by a least-squares fit to $y_D(2\theta)$. Then

$$K=A_0[N_v(1+I_M/\langle I_1\rangle)\langle I_1\rangle]^{-1},$$
$$\alpha_i=\frac{(1+I_M/\langle I_1\rangle)\langle I_1\rangle}{M_{Cu}M_{Ni}(\bar{b}_{Cu}-\bar{b}_{Ni})^2}\frac{A_i+B_i}{C_iA_0}, \tag{15}$$
$$\beta_i=\frac{(1+I_M/\langle I_1\rangle)\langle I_1\rangle}{M_{Cu}M_{Ni}(\bar{b}_{Cu}-\bar{b}_{Ni})^2}\frac{B_i}{C_iA_0}.$$

RESULTS AND DISCUSSION

Room-temperature patterns of the cluster scattering, such as in Fig. 1, were run on both single sheets of sample and on the two sheets together at a wavelength of 1.024 Å. The incident beam was monochromated by using the (311) planes of a germanium single crystal, thus eliminating $\frac{1}{2}\lambda$ contamination. The angular resolution determined by a standard Al_2O_3 powder gave widths at half-maximum of 0.40°, 0.40°, 0.41°, 0.44°, and 0.50° at 20°, 30°, 40°, 50°, and 60° scattering angles. The air scattering with no sample in the beam was multiplied by $\exp(-\tau\sec\theta)$. After subtracting the corrected air scattering these data were also corrected to normal incidence and unit transmission. The τ's appropriate to the sample thickness and wavelength were used. The data were taken for a preset incident beam monitor count of 8×10^6. The scattering data from each single thickness of sample, one consisting of 187 data points and the other of 116 points, and of the two thicknesses together with 177 data points were analyzed using Eqs. (14) to least-squares fit the data. The least-squares fitting was repeated with an increasing number of unknowns, starting with K only and proceeding until the first nine α's and β_1 were included. In Table II the sum of the proportionality constants for the two single-thickness patterns, K_1+K_2, and the proportionality constant for the two thicknesses together, K_{1+2}, against N, the number of unknowns, are tabulated. If the correction for the multiple scattering is proper, then by Eq. (13), $K_1+K_2=K_{1+2}$. Examination of the table shows that this criterion is satisfied for all K's in the table to better than 1%, indicating a satisfactory correction for the multiple scattering.

Because the vertical divergence used for the customary scattering angles (15° to 90°) were too large to ensure that the small-angle scattering would not suffer instrumental distortions, data were also taken with special slits and at larger wavelength. The (111) planes of the germanium monochromator were used to produce a beam of 1.951 Å neutrons. The special slits consisted of a collimator before the sample with a horizontal and vertical divergence of ±0.095° and a collimator before the counter with a horizontal divergence of ±0.130° and a vertical divergence of ±0.609°. Because a spread in incident wavelength does not produce a serious loss in resolution at small angles, and more intensity was needed, the in-pile collimator before the monochromator was removed. Both patterns, at 1.024 Å and at 1.951 Å,

[30] G. E. Bacon, *Neutron Diffraction* (Oxford University Press, London, 1962), p. 57.

TABLE II. Sum of the proportionality constants for the two single-thickness patterns and the proportionality constant for the two thicknesses together in units of 10^{-5}, against N, the number of unknowns.

N	1	2	3	4	5	6	7	8	9	10	11
(K_1+K_2)	2.7300	2.5726	2.5734	2.5741	2.5743	2.5743	2.5745	2.5744	2.5743	2.5743	2.5739
K_{1+2}	2.7091	2.5954	2.5966	2.5968	2.5968	2.5968	2.5968	2.5970	2.5969	2.5969	2.5969

were stepped in increments of $\lambda^{-1}\sin\theta$. Because the multiple scattering is a function of the total cross section σ_T in Eq. (2), the two patterns could not be joined together by simply scaling the 1.951 Å data to match the 1.024 Å data. Instead, the value of the minimum occurring at $\lambda^{-1}\sin\theta\sim0.146$ in each data set (see Fig. 1) was subtracted from the respective data. The areas under these two sets of reduced data were found by numerical integration over the region of the abscissa in Fig. 1 labeled "fit." The reduced 1.951 Å data were then multiplied by the ratio of the areas of the 1.024 Å to the 1.951 Å reduced data, and the value of the minimum of the 1.024 Å data was added to the product. The resulting data match was excellent. In Fig. 1 the pluses are the matched 1.951 Å data. The matched data were then treated as if all data were taken at 1.024 Å. In least-squares fitting Eq. (14) to these data the matched points of the 1.951 Å data up to the point "stop 2" in Fig. 1 were used, while the 1.024 Å data were used starting at the point labeled "start 1" and beyond. The positions of the Bragg reflections are indicated in Fig. 1 and those points indicated by the crosses were deleted from the least-squares analysis as being part of a Bragg reflection. The least-squares fitting was repeated, increasing the number of unknowns by one, starting with α_1 and proceeding until a total of nine α's and five β's were included. The results are presented in Table III. The first nine columns are the α's for shells one through nine, and columns ten through fourteen are the first β's for shells one through five. The coordination numbers C_i are also given. The last column is the standard deviation σ_y in counts. Examination of the table shows that the parameters do not change value appreciably as further unknowns are added, the exception being the parameter immediately preceding the added parameter. Very little improvement in the standard deviation results from including more than about seven or eight unknowns. A standard deviation of 318 is four times the standard deviation in a point due to counting statistics. Since the average first-order scattering is largely $M_{\mathrm{Cu}}N_{\mathrm{Ni}}(\bar{b}_{\mathrm{Cu}}-\bar{b}_{\mathrm{Ni}})^2$, it is seen from Eq. (15) that the relative error in the α's or β's is that in $(1+I_M/\langle I_1\rangle)$, or $\sim\pm1.2\%$. Having determined K_{1+2}, there is a consistency check on the values taken for the scattering lengths. Using Eqs. (11) and (12) and the (111) reflection, we measure a mean scattering length of $(0.0415\pm0.0046)\times10^{-12}$ cm, while that computed from the scattering lengths and composition is $(0.0183\pm0.0148)\times10^{-12}$ cm.

An attempt was made to measure the possible ferromagnetic scattering in the (111) reflection at 2 and 4°K. In this case $F_{hkl}^2=F_N^2+\frac{2}{3}F_M^2$, where F_N is the nuclear structure factor and F_M is the magnetic structure factor. Assuming that $F_M=4(M_{\mathrm{Cu}}\times0+M_{\mathrm{Ni}}p)$, we estimate $p_{111}=(0.000\pm0.060)\times10^{-12}$ cm. Mook[19] gives $p_{111}=0.123\times10^{-12}$ cm for pure nickel. Since it is to be expected that p for our alloy would be smaller than for elemental nickel,[20] magnetic effects in our sample were too small to have been detected within the accuracy of our measurements.

The probability of finding a B atom at a distance r_i from any given B atom is $M_B+M_A\alpha_i$. Since α_1 is positive, it is more likely that atoms will be found in the first-neighbor shell, like the origin atom. Thus, the probability of finding a nickel atom in the first-neighbor shell around a nickel atom increases from the random probability of 0.475 to 0.539. This clustering is most pronounced for the first-neighbor shell, and in fact the solid solution is essentially random beyond this shell. If the first-neighbor size-effect coefficient is significant, then Eq. (9) gives $1.226\epsilon_{\mathrm{CuCu}}{}^1+1.084\epsilon_{\mathrm{NiNi}}{}^1=-0.00062$. If we assume that the Cu-Cu and Ni-Ni distances in our alloy are the same as in the pure elements,[31] we would compute $1.226(+0.0071)+1.084(-0.0181)=-0.0109$. Thus the sign of the experimental effect is correctly predicted by such a crude assumption. However, these results lead to the conclusion that the elastic strain energy in our alloy is negligibly small.

The clustering is, of course, dependent upon the temperature of the alloy. The thermal history of the sample was described under "Sample Preparation." Figure 2 shows scattering patterns obtained in 24-h furnace runs at 25, 329, 750, and 1021°C. There is a definite decrease in Δ, the difference in the maximum M and minimum m of the cluster scattering, as the temperature is raised. However, there are two effects producing this decrease: the diminution in the clustering and the change in the Debye parameter $2B$ of Eq. (6). Assuming that the cluster scattering is due mainly to the first neighbors, we write

$$\frac{\Delta(T)}{\Delta(25°\mathrm{C})}=\frac{\alpha_1(T)}{\alpha_1(25°\mathrm{C})}f(T), \tag{16}$$

where

$$f(T)=\frac{\{[e^{-2B\gamma_1[(\sin\theta)/\lambda]^2}(\sin\kappa r_1)/\kappa r_1]_M-[e^{-2B\gamma_1[(\sin\theta)/\lambda]^2}(\sin\kappa r_1)/\kappa r_1]_m\}_T}{\{[e^{-2B\gamma_1[(\sin\theta)/\lambda]^2}(\sin\kappa r_1)/\kappa r_1]_M-[e^{-2B\gamma_1[(\sin\theta)/\lambda]^2}[(\sin\kappa r_1/\kappa r_1]_m\}_{25°\mathrm{C}}}.$$

[31] *International Tables for X-Ray Crystallography III* (Kynoch Press, Birmingham, England, 1962), Table 4.3.

TABLE III. Short-range order and size-effect parameters. α and β are the short-range order and size-effect parameters, C is the coordinate number, and σ_y is the standard deviation.

α_1 $C_1=12$	α_2 $C_2=6$	α_3 $C_3=24$	α_4 $C_4=12$	α_5 $C_5=24$	α_6 $C_6=8$	α_7 $C_7=48$	α_8 $C_8=6$	α_9 $C_9=36$	β_1 $C_1=12$	β_2 $C_2=6$	β_3 $C_3=24$	β_4 $C_4=12$	β_5 $C_5=24$	σ_y counts
+0.1309														489
+0.1203	+0.0366													427
+0.1219	−0.0079	+0.0149												327
+0.1218	−0.0065	+0.0114	+0.0087											322
+0.1218	−0.0065	+0.0113	+0.0096	−0.0005										321
+0.1219	−0.0066	+0.0113	+0.0103	−0.0028	+0.0074									320
+0.1219	−0.0068	+0.0114	+0.0103	−0.0024	−0.0032	+0.0019								319
+0.1219	−0.0070	+0.0114	+0.0103	−0.0024	−0.0042	+0.0027	−0.0062							318
+0.1220	−0.0071	+0.0114	+0.0106	−0.0026	−0.0038	+0.0025	+0.0048	−0.0018						318
+0.1214	−0.0055	+0.0113	+0.0103	−0.0024	−0.0036	+0.0023	+0.0051	−0.0018	−0.0003					317
+0.1211	−0.0060	+0.0116	+0.0103	−0.0025	−0.0037	+0.0024	+0.0048	−0.0018	−0.0003	−0.0003				317
+0.1211	−0.0078	+0.0113	+0.0118	−0.0025	−0.0033	+0.0023	+0.0046	−0.0017	−0.0003	−0.0004	−0.0002			316
+0.1210	−0.0080	+0.0106	+0.0117	−0.0016	−0.0034	+0.0023	+0.0050	−0.0017	−0.0003	−0.0004	−0.0002	−0.0003		315
+0.1210	−0.0083	+0.0103	+0.0098	−0.0014	+0.0006	+0.0023	+0.0039	−0.0016	−0.0003	−0.0004	−0.0003	−0.0005	−0.0002	315

If we assume the usual temperature dependence[32] for B, we can estimate the decrease in $\alpha_1(T)$ with temperature. The parameters and results are summarized in Table IV. The value of α_1 at 25°C is representative of the clustering at ~550°C, as will be clarified next.

There then remains the consideration of the temperature of the alloy for which the parameters in Table III are representative after furnace cooling from 1021°C. The time for an atom in a fcc lattice to jump to any one of its 12 neighbors is an important parameter. This time is approximately $\tau_1 \cong a_0^2/D$, where a_0 is the lattice constant and D is the diffusion constant. Monma *et al.*[33] have recently measured the nickel diffusion rate using the tracer method with Ni^{63} in the alloy 54.6%Ni–45.5%Cu, which is close to our composition. They find $D_0=17.0$ cm^2 sec^{-1}, and $Q=66.8$ kcal mole^{-1} in the range 985 to 1210°C. By extrapolating their result to lower temperature we calculate the following jump times: 500°C—500 sec, 600°C—4 sec, 700°C—0.07 sec, and 1021°C—10^{-5} sec. It is obvious that no cooling rate will quench the local atomic arrangements at 1021°C. On the other hand, almost any reasonable cooling rate, such as the furnace cooling in our experiment, will prevent changes below 500°C. We actually require from one to ten jumps to get close to an equilibrium arrangement. We can put these arguments into a more quantitative statement. Let τ_n = the time to make n jumps. Then when

$$(d\tau_n/dT)(dT/dt)=1, \tag{17}$$

where (dT/dt) is the quenching rate, we have the condition for quenching, namely, the amount of time available during cooling is sufficient to make n jumps. Above the temperature defined by Eq. (17) there is more than enough time to make n jumps, whereas below that temperature there is insufficient time. We have

$$d\tau_n/dT=-na_0^2Qe^{Q/RT}/RT^2D_0, \tag{18}$$

where R is the gas constant. Using Monma's values for Q and D_0 and our measured quenching rate, we have plotted $(1/n)(d\tau_n/dT)(dT/dt)$ versus $1/T$ in Fig. 3. The graph allows one to read quickly the quench temperature; for $n=1$, it is 547°C, and for $n=10$, it is 597°C. These temperatures represent the probable bounds on the temperature representative of our measurements in Table III.

These results of a large clustering effect in CuNi mean that the lowest-energy state of the alloy, at 0°K, will be fully phase-separated into pure copper and pure nickel. Above 0°K there will be a critical temperature T_c whose maximum is ideally located at 50 at.% nickel, and which falls off symmetrically with composition in a way identical to a classical coherent spinodal.[34] A

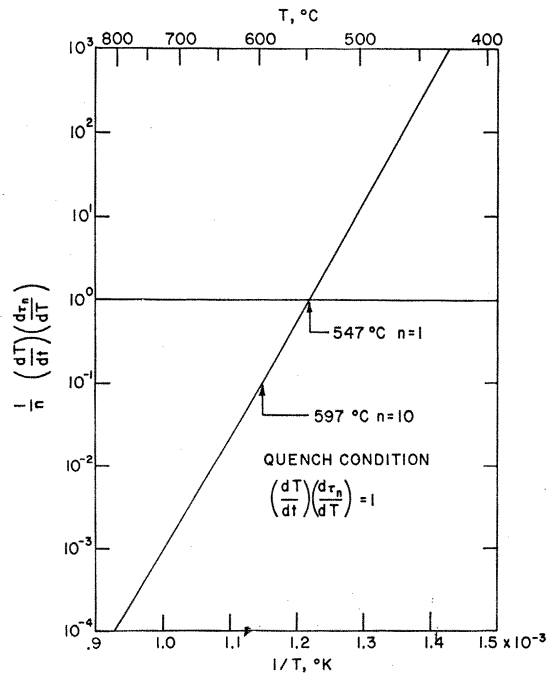

FIG. 3. Plot of $(1/n)(d\tau_n/dT)(dT/dt)$ versus $1/T$. The probable limits of the quench temperature are indicated.

[32] *International Tables for X-Ray Crystallography II* (Kynoch Press, Birmingham, England, 1962), p. 233.

[33] K. Monma, H. Suto, and H. Oikawa, J. Japan Inst. Metals **28**, 188 (1964).

[34] J. W. Cahn, Acta Met. **9**, 795 (1961).

TABLE IV. Approximate change in α_1 with temperature. At 25°C, $\alpha_1=+0.121$ is representative of ~550°C.

T(°C)	$2B\gamma_1$	$f(T)$	$\Delta(T)$ counts	$\frac{\Delta(T)}{\Delta(25)}$	$\frac{\Delta(T)}{\Delta(25)f(T)}$	α_1 (expt)	α_1 (theory)
25	0.7193	1.0000	1337	1.0000	1.0000	+0.121	+0.120
329	1.4078	0.9710	1349	1.0090	1.0392	+0.126	···
750	2.3792	0.9315	1018	0.7614	0.8174	+0.099	+0.092
1021	3.0066	0.9071	881	0.6589	0.7264	+0.088	+0.068

spinodal describes the locus of points, in the absence of elastic-energy contributions, for which the second derivative with respect to composition of the Gibbs free energy $\partial^2G/\partial C^2$ is zero. It is at the boundary of the spinodal, within the associated miscibility gap, that the solid solution first becomes unstable to infinitesimal composition fluctuations and begins to phase-separate. Such phenomena can be described by statistical theories based on the Ising model which treat order-disorder transformations (or antiferromagnetism) and phase separation (or ferromagnetism).

Of the available approximate theories of pair correlations in binary alloys, the one most tractable for an arbitrary range of interaction is that developed recently by Clapp and Moss.[35] This theory is essentially the alloy counterpart of the linearized mean-field approximation for the spin-spin correlations in an Ising magnet above T_c. Brout[36] has suggested that such a theory becomes valid for $|T-T_c|/T_c>1/C_1$ ($C_1=12$ for fcc). The essentials of the theory are given by Eqs. (32)–(35) of Ref. 35. The measured short-range order parameters are related to the pairwise interactions through

$$\alpha_{0i}=-\frac{2M_{\mathrm{Cu}}M_{\mathrm{Ni}}}{kT}\sum_j V_{0j}\alpha_{ji}, \qquad (19)$$

in which the correlation α_{0i} between the origin site 0 and the ith neighbor is written in terms of the sum over the product of the interaction energies V_{0j} between the origin and the j neighbors of i, and the correlations α_{ji} between j and i. The energies V_{0j} are the familiar pairwise combinations

$$V_{0j}=\tfrac{1}{2}(V_{0j}^{\mathrm{CuCu}}+V_{0j}^{\mathrm{NiNi}})-V_{0j}^{\mathrm{CuNi}}. \qquad (20)$$

We may simplify notation by writing V_1 if 0 and j are nearest neighbors, V_2 if they are second, etc. Similarly, we write α_1 if 0 and j are nearest neighbors, α_2 if they are second, etc. If $V_1>0$, unlike nearest pairs will be preferred and the ground state of the system will tend toward order. Similarly, if $V_1<0$, the ground state will tend toward phase separation.

The system of linear equations in Eq. (19) can be diagonalized and solved for the intensity of the diffuse scattering, and thus by Fourier inversion, for the α's. The critical temperature enters into this procedure as the temperature at which the diffuse intensity tends to infinity at a reciprocal-lattice point. In our case, for a clustering system, this is at any fundamental reciprocal-lattice point including the origin. These considerations lead to the following expression for T_c[37]:

$$T_c=-(6V_1/k)[1+\tfrac{1}{2}V_2/V_1+2V_3/V_1\cdots]. \qquad (21)$$

It is necessary to use interactions at least to second neighbors to fit our experimental results. For first- and second-neighbor interactions only, it can be shown[37] that the conditions for clustering are $V_1<0$ and $-1.0<V_2/V_1<+\infty$. The parameters in Eq. (19) were put in terms of T_c/T and V_2/V_1, where $547°C<T<597°C$. A wide range of T_c/T (from 0.250 to 0.900) and V_2/V_1 (from -0.950 to $+15.00$) were used in a computer program to generate a set of α's that would match the measured values in Table III.

Table V lists those computer results in reasonable agreement with our experimental α's. The first eight columns are sets of computed α's for the T_c/T and V_2/V_1 values at the top of the column, while the last column is our best experimental values. The best agreement was in the ranges $0.675<T_c/T<0.750$ and $-0.650<V_2/V_1<-0.550$. For $V_2/V_1>0$, all the α's were positive and α_1 was too small. Thus a large positive V_2 opposite in sign to V_1 is required to match the experimental results. This finding indicates the probable importance of higher-neighbor interactions as well. That such a set of interaction energies produce a large first-neighbor parameter α_1 and small values for all other α_i can be understood by examining the arrangement of neighbors. Second neighbors of the origin atom share four first neighbors with that origin and their occupancy is determined by a balance between V_1 and V_2. V_2 requires unlike second neighbors, while V_1 demands that the first neighbors of the origin atom have in turn like first neighbors of themselves. This competition propagates to higher neighbors as well and tends to reduce all order parameters, save α_1, to small values. The best agreement in Table IV is for $T_c/T=0.725$ and $V_2/V_1=-0.600$. This satisfies Brout's criterion[36] of theoretical validity since $|T-T_c|/T_c\simeq 0.38$. With $547°C<T<597°C$, then, via Eq. (21), $322°C<T_c<358°C$, $-0.0130\text{ eV}<V_1<-0.0122\text{ eV}$, and $0.0073\text{ eV}<V_2<0.0078\text{ eV}$. Our statistical prediction of the critical temperature must be reconsidered since it is known that approximate theories predict too high a critical temperature. While the agreement in terms of

[35] P. C. Clapp and S. C. Moss, Phys. Rev. **142**, 418 (1966).
[36] R. H. Brout, *Phase Transitions* (W. A. Benjamin, Inc., New York, 1965), p. 25.
[37] P. C. Clapp and S. C. Moss, Phys. Rev. **171**, 754 (1968).

TABLE V. Calculated short-range order parameters for selected values of T_c/T and V_2/V_1 compared with experimental values.

T_c/T	0.675	0.675	0.700	0.700	0.725	0.725	0.750	0.750	Experiment
V_2/V_1	−0.550	−0.600	−0.600	−0.650	−0.600	−0.650	−0.600	−0.650	
α_1	+0.104	+0.110	+0.113	+0.117	+0.120	+0.124	+0.127	+0.131	+0.121
α_2	−0.009	−0.018	−0.011	−0.016	−0.009	−0.014	−0.006	−0.011	−0.008
α_3	+0.014	+0.014	+0.016	+0.016	+0.018	+0.018	+0.021	+0.021	+0.010
α_4	+0.013	+0.016	+0.016	+0.018	+0.018	+0.019	+0.020	+0.022	+0.010
α_5	−0.002	−0.005	−0.003	−0.005	−0.003	−0.004	−0.002	−0.004	−0.002
α_6	+0.003	+0.002	+0.003	+0.003	+0.004	+0.003	+0.004	+0.004	+0.002
α_7	+0.002	+0.002	+0.002	+0.003	+0.003	+0.003	+0.004	+0.004	+0.002
α_8	−0.001	−0.001	−0.001	−0.001	−0.001	−0.001	−0.001	−0.001	+0.004
α_9	−0.001	−0.001	−0.001	−0.002	−0.001	−0.002	−0.001	−0.002	−0.002

T_c/T may be quite good, the predicted T_c may be 10–15% too high and is definitely an upper limit.[37] Assuming our theory is in error by 15%, we estimate $233°C < T_c < 263°C$.

For calculating the theoretical values of α_1 as a function of temperature in Table IV, the uncorrected estimate of $T_c = 350°C$ should be used, and the values for α_1 so determined are listed in the table. One of the interesting aspects of the temperature dependence of the short-range order parameters is that α_2 becomes more negative as the temperature is increased, indicating the increasing influence of V_2. This is readily apparent from examination of Table V. This fact means that the relative contribution of α_2 to $\Delta(T)$ increases with increasing temperature, which makes the experimental α_1 in Table IV appear larger than is actually the case.

Rapp and Maak,[5] by extrapolating their activity data and the heats of mixing of Oriani and Murphy, made a rough prediction of the miscibility gap in CuNi which had a maximum of 300°C between 70 and 80 at.% nickel. We have recalculated this gap both to check their prediction and to obtain an estimate of T_c for our composition. We used the relation

$$\Delta H^M = \partial(\Delta G^M/T)/\partial(1/T), \qquad (22)$$

with the assumption that the enthalpy of mixing, ΔH^M, is not a function of temperature. The free energy of mixing, ΔG^M, was taken from the data of Rapp and Maak[5] at 700°C and values of ΔH^M were taken from the 640°C measurements of Oriani and Murphy.[4] Integration of Eq. (22) gives ΔG^M for any temperature and permits the calculation of both the miscibility gap and the spinodal. The calculation is more reliable for the copper-rich end of the phase diagram. The resulting miscibility gap has a maximum at 310°C at 70 at.% nickel and falls off rapidly at higher nickel concentrations and more slowly with increasing copper concentration. The spinodal is very approximately 200°C at our composition.

It is not surprising that phase separation has never been observed in Cu-Ni alloys. T_c is so low that impossibly long annealing times are required to produce decomposition on a scale observable by optical microscopy. Electron microscopy, electron diffraction, or x-ray diffraction would never resolve even small scale effects since the scattering powers of the two elements are nearly the same. Indeed, it is through the fortuitous choice of our alloy that these neutron results provide the first direct evidence of clustering in the Cu-Ni alloy system.

ACKNOWLEDGMENTS

The authors would like to thank A. Cinquepalma for his assistance in the instrumentation. We are indebted to Dr. W. C. Koehler for his advice on the best scattering lengths of the nickel isotopes and to Dr. H. Meister for assistance in measuring our alloy cross sections. We also wish to thank Professor J. W. Cahn for discussions of the spinodal mechanism and thermodynamics of the Cu-Ni system, and Dr. P. C. Clapp for his valuable discussions.